

The fully kinetic Biermann battery and associated generation of pressure anisotropy

K. M. Schoeffler,¹ N. F. Loureiro,² and L. O. Silva¹

¹*GoLP/Instituto de Plasmas e Fusão Nuclear, Instituto Superior Técnico,
Universidade de Lisboa, 1049-001 Lisboa, Portugal*

²*Plasma Science and Fusion Center, Massachusetts Institute of Technology, Cambridge MA 02139, USA*
(Dated: March 12, 2022)

The dynamical evolution of a fully kinetic, collisionless system with imposed background density and temperature gradients is investigated analytically. The temperature gradient leads to the generation of temperature anisotropy, with the temperature along the gradient becoming larger than that in the direction perpendicular to it. This causes the system to become unstable to pressure anisotropy driven instabilities, dominantly to electron Weibel. When both density and temperature gradients are present and non-parallel to each other, we obtain a Biermann-like linear in time magnetic field growth. Accompanying particle in cell numerical simulations are shown to confirm our analytical results.

Introduction. Both the seed field required for the generation of astrophysical magnetic fields [1, 2] and intense magnetic fields generated in laser-solid interaction laboratory experiments [3–6] have been attributed to the Biermann battery [7]. The Biermann battery mechanism generates magnetic fields due to non-parallel temperature and density gradients. Until now, the understanding of this mechanism has been restricted to fluid models where an extra non-ideal term is added to Ohm’s law. In weakly or non-magnetized plasmas, the validity of fluid models rests on collisions being sufficiently frequent compared to the dynamic timescales of the problem, such that the pressure tensor remains in scalar form [8]. These conditions are often not present in astrophysical environments and are questionable in some laser-plasma environments, and thus a fully kinetic model is necessary.

Recently, the Biermann battery has been investigated with fully self-consistent kinetic 3D simulations [9, 10], but a clear theoretical model for how the fully kinetic Biermann battery actually works in collisionless plasmas has not been presented. Such a model is presented here for the first time, explaining not only the kinetic Biermann battery but also, more generally, the dynamical evolution of collisionless unmagnetized plasmas subject to background density and temperature gradients. In addition to extending the validity of the Biermann battery to many weakly collisional scenarios, we reveal the purely kinetic result that a temperature gradient alone leads to the generation of anisotropies in temperature (pressure tensor). This anisotropy gives rise to kinetic instabilities such as the Weibel instability [11], seen in [9, 10], or instabilities that inhibit the heat flux [12, 13] on time scales short compared to the collision time. This is relevant for a wide variety of settings including astrophysical shocks and laser experiments with small collision rates, and aids in the understanding of cooling flows in galaxy clusters, which cannot be explained assuming the larger heat flux predicted based solely on collisions [14].

Model. We solve the time evolution of the velocity distribution function and electromagnetic fields accord-

ing to the coupled Vlasov and Maxwell’s equations, assuming that only the electrons play a role and the ions are static, only acting as a neutralizing background. For our calculation, we normalize the velocity \mathbf{v} to $v_{T0} \equiv \sqrt{T_e/m_e}$, time t to ω_{pe}^{-1} , and \mathbf{x} to λ_D , where ω_{pe} is the plasma frequency for density $n = n_0$, and $\lambda_D \equiv v_{T0}/\omega_{pe}$ is the Debye length. In addition E and B are normalized to $E_0 \equiv m_e v_{T0} \omega_{pe}/e$ and $B_0 \equiv m_e c \omega_{pe}/e$ respectively.

We will assume that a background Maxwellian distribution function, f_M , is instantaneously perturbed such that

$$n = n_0 (1 + \epsilon x), \quad v_T = v_{T0} \sqrt{1 + \delta y}, \quad (1)$$

$$\epsilon \equiv \frac{\lambda_D}{L_n} \equiv \lambda_D \frac{1}{n} \frac{\partial n}{\partial x}(0), \quad \delta \equiv \frac{\lambda_D}{L_T} \equiv \lambda_D \frac{1}{T} \frac{\partial T}{\partial y}(0). \quad (2)$$

This perturbation is not an equilibrium solution; it will be taken as a given initial state. Note that the Biermann battery is not an instability (in fluid models it grows linearly, not exponentially, with time; we will find here that this remains true in the kinetic case). As such, it has to arise from a non-equilibrium state.

The parameters ϵ and δ are taken to be very small and comparable to each other; they will be used as our asymptotic expansion coefficients. Assuming $\mathbf{x} \sim \epsilon^0$, the initial distribution function to second order in ϵ and δ is:

$$\begin{aligned} f_0 = & f_M + \epsilon x f_M - \frac{1}{2} \delta y (3 - v^2) f_M \\ & + \frac{1}{8} \delta^2 y^2 (15 - 10v^2 + v^4) f_M - \frac{1}{2} \epsilon \delta x y (3 - v^2) f_M. \end{aligned} \quad (3)$$

We evolve the Vlasov-Maxwell equations initialized with this distribution function, and either no initial electric or magnetic fields, or natural equilibrium fields that act to balance the force due to the pressure gradient.

The evolution of the electron distribution function subject to these density and temperature gradients is given

by the Vlasov equation, coupled with Faraday's and Ampere's laws:

$$\frac{\partial f}{\partial t} + \mathbf{v} \cdot \nabla f - (\mathbf{E} + \mathbf{v} \times \mathbf{B}) \cdot \nabla_v f = 0, \quad (4)$$

$$\frac{\partial \mathbf{B}}{\partial t} = -\nabla \times \mathbf{E}, \quad (5)$$

$$\frac{\partial \mathbf{E}}{\partial t} = \int d^3v \mathbf{v} f + \frac{c^2}{v_{T0}^2} \nabla \times \mathbf{B}. \quad (6)$$

We will seek solutions to these equations in powers of ϵ and δ . We will assume $t \sim \mathbf{x} \sim c^2/v_{T0}^2 \sim \epsilon^0 \sim \delta^0$. Although the solution is only valid when $\mathbf{x} \sim \epsilon^0$, at an arbitrary position \mathbf{x} , the calculation remains valid in a new coordinate system \mathbf{x}' , where the assumptions are satisfied using ϵ' calculated with the local v_{T0}' and n_0' . There are three other small parameters besides ϵ and δ ; namely c_s/v_{T0} , v_{T0}^2/c^2 , and ν/ω_{pe} , where c_s is the sound speed, and ν is the collision frequency. Each of these parameters are assumed to be much smaller than one, but aside from ν/ω_{pe} , can in principle remain of order ϵ^0 . [15] We implicitly assume small values for these parameters by assuming static ions, using the non-relativistic Vlasov equation/ Maxwellian distribution, and ignoring collisions.

First we highlight some important aspects of the form of the solution. The first order ($\sim \epsilon^1$) solution including all terms proportional to c_s/v_{T0} and v_{T0}^2/c^2 , of \mathbf{E} , and f is uniform in space, and f is an odd function of v . A proof of this is provided in the supplementary materials. Given a uniform E , from Eq. (5) no magnetic field is generated, and an odd f with respect to v only leads to uniform bulk flows and temperature fluxes. It is thus necessary that we perform our calculation with second order terms ($\sim \epsilon^2$) to see the Biermann battery, and the formation of a temperature anisotropy. The second order solution is different in form, and except for terms of f which are even in v , there are no terms that are uniform in space. It should be emphasized that this means that modifications coming from c_s/v_{T0} and v_{T0}^2/c^2 can be separately neglected for both first order and second order solutions. Note that second order modifications to the first order solution are then neglected (the entire solution is not accurate to ϵ^2).

Solutions can be found from an initial condition by taking an expansion for small t , restricted to second order in ϵ . Fortunately, the sum over all orders of t converges to a solution valid for arbitrary $t \sim \epsilon^0$, and thus only small compared to the electron transit time $L_T/v_{T0} = \delta^{-1}$.

Density gradient. We first consider the case with only a density gradient ($\delta = 0$). If we assume the initial condition of $f = f_0$ and no initial electric or magnetic fields, we obtain the following analytic solution:

$$f = f_0 + \tilde{f}_n(t), \quad (7)$$

$$\mathbf{E} = -(\epsilon - \epsilon^2 x) [1 - \cos(\omega_{pe,x} t)] \hat{\mathbf{x}}, \quad (8)$$

where $\omega_{pe,x} \equiv 1 + \epsilon x/2$ is the normalized plasma frequency based on the x dependent density, n , and \tilde{f}_n is an oscillatory term described in the supplementary materials. It is evident that the electric field of this solution oscillates about

$$\mathbf{E} = -(\epsilon - \epsilon^2 x) \hat{\mathbf{x}}. \quad (9)$$

The space dependent frequency, $\omega_{pe,x}$, gives rise to increasingly shorter scale x variations of the electric field. These variations along x lead to phase mixing in space and then Landau damping. Our model does not show this damping because the damping is exponentially suppressed until $k\lambda_D \lesssim 1$ which occurs at $t \sim \epsilon^{-1}$ where the assumptions break down. Eventually Landau damping eliminates the oscillations, and thus the electric field should naturally settle to Eq. (9). If we take Eq. (9) as the initial condition for the electric field, we arrive at an equilibrium solution to Eqs. (4–6) where \mathbf{E} and f do not change with time.

Temperature gradient. We now consider a second case, with a temperature gradient only ($\epsilon = 0$, $\delta \neq 0$). If we again start with the initial conditions $f = f_0$, and no initial electric or magnetic fields, to second order in δ , the solution to Eqs. (4–6) is the following:

$$f = f_{\nabla T} + \tilde{f}_T(t), \quad (10)$$

$$\mathbf{E} = -\delta [1 - \cos(t)] \hat{\mathbf{y}}, \quad (11)$$

where

$$\begin{aligned} f_{\nabla T} \equiv & f_0 + \frac{1}{2} \delta t v_y (5 - v^2) f_M \\ & - \frac{1}{4} \delta^2 t y v_y (25 - 12v^2 + v^4) f_M \\ & + \delta^2 t^2 \left[\frac{1}{8} v_y^2 (39 - 14v^2 + v^4) - \frac{1}{4} (5 - v^2) \right] f_M, \end{aligned} \quad (12)$$

and \tilde{f}_T is an oscillatory term described in the supplementary materials. Once again the solution oscillates around a particular value for the electric field:

$$\mathbf{E} = -\delta \hat{\mathbf{y}}. \quad (13)$$

Although Landau damping at the gradient scale with a wavelength $k\lambda_D \sim \delta$ is exponentially suppressed, in a system with density gradients, this field would also Landau damp as described earlier. Therefore it is similarly natural to consider starting from Eq. (13) as the initial condition. This yields a simpler solution where the electric field is constant with time, but the distribution function continues to evolve with time as $f = f_{\nabla T}$.

Two important terms in Eq. (12) grow with t and eventually break the assumptions of the ordering. The second

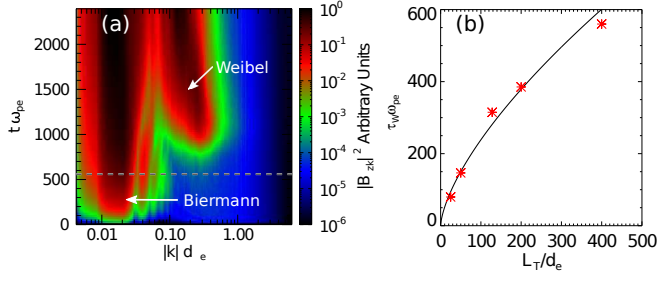


FIG. 1. (a) Magnetic energy spectra of B_z (with respect to $|k| = \sqrt{k_x^2 + k_y^2}$) vs. time from the simulation with system size $L_T/d_e = 400$ ($L_T/\lambda_D = 2000$) reported in Ref. [9]. The time when the Weibel instability begins to grow exponentially is identified with a dashed line. This estimate of the onset time τ_W is plotted vs. system size (b) along with the predicted curve where Eq. (16) is satisfied indicating where the Weibel growth rate exceeds that of the anisotropy predicted in Eq. (15).

term on the RHS of Eq. (12) is associated with the heat flux, and matches the collisional solution shown in [12] once t reaches the collision time. However the assumptions will have already broken when $t \sim \delta^{-1}$. The fourth term on the RHS of Eq. (12), which grows as t^2 is associated with a temperature anisotropy, where the collisionless temperatures in each direction (corresponding to diagonal components of the pressure tensor) differ. This term breaks the assumptions earlier; when $t \sim \delta^{-1/2}$ (a hybrid between the plasma period and electron transit time $(L_T/v_{T0}\omega_{pe})^{1/2}$). However, the simulations will show that the predictions remain valid beyond this limit.

We define the pressure tensor (normalized to $m_e n_0 v_{T0}^2$) as:

$$nT_{ij} \equiv \int d^3v v_i v_j f, \quad (14)$$

from which we find $T_{yy} = v_T^2 + 3/2\delta^2 t^2$ and $T_{xx} = T_{zz} = v_T^2 + 1/2\delta^2 t^2$, resulting in the following anisotropy:

$$A \equiv \frac{T_{yy}}{T_{xx}} - 1 = \delta^2 t^2. \quad (15)$$

The temperature gradient thus naturally leads to a temperature anisotropy. More energetic particles up the gradient arrive faster if their momentum is predominantly along the gradient. This anisotropy will give rise to kinetic instabilities such as the Weibel instability [11] seen in [9] or instabilities that inhibit the heat flux [12, 13].

Eq. (15) is consistent with the anisotropy and the subsequent development of the Weibel instability obtained in the PIC simulations reported in [9] — see Fig. 1. The onset time of the Weibel instability τ_W is roughly estimated from the magnetic energy spectra when the Weibel field begins to grow exponentially. Fig. 1(a) shows the

spectra for the case where $L_T/d_e = 400$ ($\delta^{-1} = 2000$), with the onset of Weibel indicated by a dashed line. Although the Biermann field is energetically dominant for smaller system sizes, the higher k Weibel instability is present (i.e. an onset time can be measured) for all simulations. The onset time, τ_W , should occur when the Weibel growth rate, which is a function of anisotropy, and thus of time, exceeds the predicted rate of anisotropy growth from Eq. (15):

$$\gamma_W(A(\delta t)) > 1/A \partial A / \partial t = 2/t. \quad (16)$$

Fig. 1(b) shows that this prediction matches the estimated onset over a range of system sizes remarkably well, where $\gamma_W(A)$ is the growth rate of the Weibel instability, given by [11], which we solve numerically. γ_W is calculated at the location of fastest growth ($x/L_T = 0.9125, y/L_T = 0$), which is independent of system size using the local values; $v_T = 0.036c$, $n = 0.12n_0$, and the anisotropy calculated from Eq. (15) using $L_{T,local} = 0.0625L_T$ and v_T . Note that this anisotropy is slightly increased by a factor of 5/4 to take into account second order variations in temperature, which will be addressed in a future work. [16]

It is surprising that the agreement is so good since these simulations are in highly nonlinear regimes; the assumption that $\tau_W \ll \delta^{-1}$ is only satisfied for sufficiently large L_T/d_e . For the largest $L_T/d_e = 400$ case ($\tau_W \omega_{pe,local} \approx 0.8\delta_{local}^{-1}$), nonlinear effects were clearly present. The thermal velocity, which we assume to be constant with time except for the small modification $\sim \delta^2 t^2$, grew as $v_T \sim t$. The measured anisotropy grew at close to $A \sim t^4$, which is still consistent with $A = \delta^2 t^2$, given that δ is now a function of time. We expect the onset time to continue to follow this trend for even larger L_T , where our assumption $\tau_W \omega_{pe,local} \ll \delta_{local}^{-1}$ is valid.

Biermann battery. Both of these simplified cases begin oscillating about the equilibrium electric fields, Eq. (9) and Eq. (13), at the timescale of the electron plasma frequency, and Landau damping eventually eliminates these oscillations. These equilibrium fields balance the associated pressure gradients. It is thus a natural assumption to start with a similar electric field for the initial conditions for the complete case ($\epsilon \neq 0, \delta \neq 0$):

$$\mathbf{E} = -(\epsilon - \epsilon^2 x + \epsilon \delta y) \hat{x} - \delta \hat{y}. \quad (17)$$

With this assumption, and starting with f_0 , the solution to Eqs. (4–6) is:

$$f = f_{\nabla T} + \frac{1}{2} \epsilon \delta t x v_y (5 - v^2) f_M + \frac{1}{2} \epsilon \delta t^2 v_x v_y f_M, \quad (18)$$

with the magnetic field:

$$\mathbf{B} = -\epsilon \delta t \hat{z}, \quad (19)$$

where the electric field does not change with time.

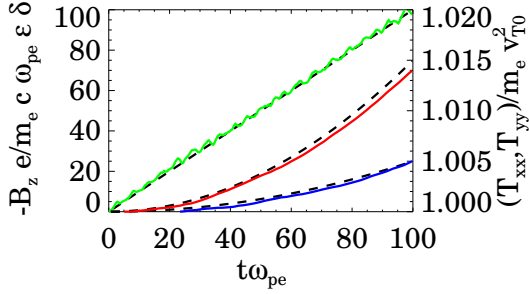


FIG. 2. Evolution of the averaged B_z due to the perpendicular density and temperature gradients (green), and anisotropic temperatures T_{xx} (blue) and T_{yy} (red), vs. time along with the predicted curves at $y = 0$ from Eq. (19) and Eq. (14) (black dashed lines).

The last term of Eq. (18) is associated with the off-diagonal component of the pressure tensor, and thus T_{xy} , which enhances the magnitude and rotates the direction of the temperature anisotropy (defined in the frame that diagonalizes T_{ij}).

We thus see a fully kinetic Biermann battery: the magnetic field grows linearly in time, and is proportional to both the density and temperature gradients, as in the fluid case.

Numerical comparison. Our analytic model has been tested via particle-in-cell (PIC) simulations using the OSIRIS framework [17, 18]. The simulations are done setting $\epsilon = \delta = 0.001$, and a normalized thermal velocity $v_{T0}/c = 0.05$, which is small such that relativistic effects do not play a role, but large compared to ϵ . A more detailed explanation of the simulation parameters and setup is outlined in the supplementary materials

To test these solutions we look at both simulations with $\delta = 0$ or $\epsilon = 0$, and with both gradients. Good agreement between the predicted and simulated electric fields for single gradients is shown in the supplementary materials. In Fig. 2 the average magnetic field from the simulation with both gradients grows linearly in time, confirming the prediction in Eq. (19). The growth of the temperatures in the x and y directions shown in Fig. 2 matches quite well with the predictions from Eq. (14). Note that our solution is rigorously only valid for $t \ll \delta^{-1/2} = 50$, but this breaking would occur at many more ω_{pe}^{-1} for realistically small values of δ that are not feasible to simulate. The plotted simulation fields are calculated by averaging the results between $-49 < x < 49$, and $-49 < y < 49$.

Conclusions. In this Letter, we have presented analytical solutions of the Vlasov-Maxwell system of equations for collisionless systems with background density and temperature gradients. The kinetic equivalent of the Biermann battery — a linear in time magnetic field growth — has been obtained for the first time. An-

other noteworthy result is the generation of temperature anisotropy in all cases where a background temperature gradient is present. This implies that pressure anisotropy driven instabilities, such as electron Weibel, should be expected in such systems. These may have a profound impact on their evolution, from effectively determining the magnetic field growth, to constraining the heat flux.

Formally the initial non-equilibrium state is taken to be generated such that the time scale for the change in temperature and density is fast compared to the electron plasma frequency. On the other hand, the time scale for the generation of these gradients, which happens for example in laser or shock interactions, is often similar or longer than the period of plasma oscillations. However, the interaction with the more slowly generated gradients would only lead to plasma oscillations comparable to those which we have shown are excited by our initial conditions. In effect, we model the time scale that is slow compared to the gradient generation, but fast compared to the electron transit time L_T/v_{T0} . Although as seen above in simulations, even when the gradients grow on the same order as L_T/v_{T0} ($\delta \propto t$) the evolution of anisotropy continues to follow Eq. (15), with $A \sim \delta(t)^2 t^2$.

It should be noted that for simplicity, there are a few limitations to the generality of this work. The pressure and density gradients are assumed to be perpendicular, and the gradients are entirely linear, not including second order variation. The more general case will be reserved for a future work.

However, this solution remains quite general. An anisotropic Maxwellian distribution ($v_{Ti0} \neq v_{Tj0}$, where v_{Ti0} is the thermal velocity in the i direction) can be modeled by the same equations. In that case, \mathbf{x} , \mathbf{v} , and \mathbf{E} are normalized using the v_{Ti0} in the same direction, and Eq. (19) has an additional factor of v_{Tx0}/v_{Ty0} . This means that the Biermann field is caused solely by the thermal spread directed along the density gradient (v_{Tx0}).

Moreover, the kinetic result of anisotropy generation is relevant even for magnetized cases, as long as there is a temperature gradient parallel to the magnetic field. Our solution for the case with $\epsilon = 0$ is valid for a uniform parallel magnetic field of arbitrary magnitude. For significantly large fields, instabilities driven by the anisotropy in a magnetized plasma, such as the firehose instability [21], would dominate over the Weibel instability.

Anisotropy driven instabilities can help explain weak heat fluxes in cooling flows. Another kinetic instability that can lead to suppression in heat flux is driven solely by the heat flux [22] with a growth rate $\gamma_{HF} \approx 0.1\Omega_{ce}\epsilon_{HF}$, where Ω_{ce} is the electron cyclotron time and ϵ_{HF} is the coefficient proportional to the heat flux taken from [22]. The second term on the RHS in Eq. (12) corresponds to $\epsilon_{HF} = \sqrt{2}\delta t$. We can estimate the onset time $\tau_{HF} \approx 2.7(\delta\Omega_{ce})^{-1/2}$ of this instability by compar-

ing the predicted heat flux growth $1/\epsilon_{HF}\partial\epsilon_{HF}/\partial t = 1/t$, to γ_{HF} .

Comparing the onset time of the heat flux instability to the Weibel $\tau_W \approx 1.6(\delta^3 v_T/c)^{-1/4}$ (in the limit $A \ll 1$, where $\gamma_W(A) = (8/27\pi)^{1/2} A^{3/2} v_T/c$ [23]), reveals the Weibel instability will appear first as long as β_e , the ratio of the electron plasma pressure to the magnetic pressure, is sufficiently large; $\beta_e \gtrsim L_T/d_e$. The Biermann battery alone often grows slow enough that β_e remains larger before the Weibel onsets; as long as $\delta \lesssim 4((v_T/c)L_n/L_T)^4$, using τ_W in Eq. (19) to find β_e . Either of these instabilities is likely to cause the heat flux to saturate long before reaching the collision time.

The purely kinetic temperature anisotropy generation from temperature gradients is thus relevant for a wide variety of settings; from astrophysical shocks and laser experiments with small collision rates where the Biermann battery can also exist, to flux tubes [19, 20] with temperature gradients found in the solar corona or at the Earth's magnetopause.

Acknowledgments. This work was supported by the European Research Council (ERC-2010-AdG Grant No. 267841, and ERC-2015-AdG Grant No. 695008). NFL was partially funded by NSF CAREER award no. 1654168.

[1] R. M. Kulsrud and S. W. Anderson, *Astrophys. J.* **396**, 606 (1992).
[2] R. M. Kulsrud and E. G. Zweibel, *Rep. Prog. Phys.* **71**, 046901 (2008).
[3] J. A. Stamper, K. Papadopoulos, R. N. Sudan, S. O. Dean, and E. A. McLean, *Phys. Rev. Lett.* **26**, 1012 (1971).
[4] C. K. Li, F. H. Seguin, J. A. Frenje, J. R. Rygg, R. D. Petrasso, R. P. J. Town, O. L. Landen, J. P. Knauer, and V. A. Smalyuk, *Phys. Rev. Lett.* **99**, 055001 (2007).
[5] G. Gregori, A. Ravasio, C. Murphy, K. Schaar, A. Baird, A. Bell, A. Benuzzi-Mounaix, R. Bingham, C. Constantin, R. Drake, M. Edwards, E. Everson, C. Gregory, Y. Kuramitsu, W. Lau, J. Mithen, C. Niemann, H.-S.

Park, B. Remington, B. Reville, A. Robinson, D. Ryutov, Y. Sakawa, S. Yang, N. Woolsey, M. Koenig, and F. Miniati, *Nature* **481**, 480 (2012).
[6] L. Gao, P. M. Nilson, I. V. Igumenshchev, M. G. Haines, D. H. Froula, R. Betti, and D. D. Meyerhofer, *Phys. Rev. Lett.* **114**, 215003 (2015).
[7] L. Biermann, *Z. Naturforsch.* **5a**, 65 (1950).
[8] In systems with large magnetic fields such that the Larmor radius is small compared to the system size (not relevant in this work) fluid models with a non-scalar pressure tensor aligned with the field can be formulated [24].
[9] K. M. Schoeffler, N. F. Loureiro, R. A. Fonseca, and L. O. Silva, *Phys. Rev. Lett.* **112**, 175001 (2014).
[10] K. M. Schoeffler, N. F. Loureiro, R. A. Fonseca, and L. O. Silva, *Phys. Plasmas* **23**, 056304 (2016).
[11] E. S. Weibel, *Phys. Rev.* **114**, 18 (1959).
[12] A. Levinson and D. Eichler, *Astrophys. J.* **387**, 212 (1992).
[13] S. P. Gary and H. Li, *Astrophys. J.* **529**, 1131 (2000).
[14] A. C. Fabian, *Annu. Rev. Astron. Astrophys.* **32**, 277 (1994).
[15] Our calculation assumes $v_{T0}^2/c^2 \sim \epsilon^0$, although as long as $\mathbf{B} \sim \epsilon^2$ (as we find in our solution), it is acceptable for $v_{T0}^2/c^2 \sim \epsilon^1$.
[16] A second derivative of the temperature, which is greater along \hat{x} , leads to a temperature anisotropy hotter along \hat{x} . ($A = t^2(\partial^2 T/\partial x^2 - \partial^2 T/\partial y^2)/T$).
[17] R. A. Fonseca, L. O. Silva, F. S. Tsung, V. K. Decyk, W. Lu, C. Ren, W. B. Mori, S. Deng, S. Lee, T. Katsouleas, and J. C. Adam, *Lect. Notes Comput. Sci.* **2331**, 342 (2002).
[18] R. A. Fonseca, S. F. Martins, L. O. Silva, J. W. Tonge, F. S. Tsung, and W. B. Mori, *Plasma Phys. Contr. Fusion* **50**, 124034 (2008).
[19] E. N. Parker, *Cosmical magnetic fields: Their origin and their activity* (Oxford, Clarendon Press; New York, Oxford University Press, 1979) p. 858.
[20] C. T. Russell, E. R. Priest, and L. C. Lee, *Physics of magnetic flux ropes* (American Geophysical Union Washington, D.C., 1990) pp. xvi, 685.
[21] E. N. Parker, *Phys. Rev.* **109**, 1874 (1958).
[22] G. T. Roberg-Clark, J. F. Drake, C. S. Reynolds, and M. Swisdak, *Astrophys. J. Lett.* **830**, L9 (2016).
[23] R. C. Davidson, D. A. Hammer, I. Haber, and C. E. Wagner, *Phys. Fluids* **15**, 317 (1972).
[24] G. F. Chew, M. L. Goldberger, and F. E. Low, *Proc. R. Soc. London, Ser. A* **236**, 112 (1956).

Supplementary Materials for: The fully kinetic Biermann battery and associated generation of pressure anisotropy

K. M. Schoeffler,¹ N. F. Loureiro,² and L. O. Silva¹

¹*GoLP/Instituto de Plasmas e Fusão Nuclear, Instituto Superior Técnico,
Universidade de Lisboa, 1049-001 Lisboa, Portugal*

²*Plasma Science and Fusion Center, Massachusetts Institute of Technology, Cambridge MA 02139, USA*

(Dated: March 12, 2022)

I. EQUATIONS SOLVED.

The evolution of the electron distribution function subject to these density and temperature gradients is given by the Vlasov equation, coupled with Faraday's and Ampere's laws, for quantities $f^{(i)}$, $E^{(i)}$, and $B^{(i)}$, which are of order $\epsilon^{(i)}$. Initially $f^{(0)} = f_M$, and $f^{(1)}$ and $f^{(2)}$ are the respective terms on the first and second lines of Eq. (3) in the paper. The initial fields are either 0, or those described in the paper in Eqs. (9, 13, 17).

The zeroth order term is trivially solved given $E^{(0)} = B^{(0)} = \nabla f^{(0)} = \int d^3v \mathbf{v} f^{(0)} / n_0 = 0$.

For the first order terms:

$$\frac{\partial f^{(1)}}{\partial t} + \mathbf{v} \cdot \nabla f^{(1)} - (\mathbf{E}^{(1)} + \mathbf{v} \times \mathbf{B}^{(1)}) \cdot \nabla_{\mathbf{v}} f^{(0)} = 0, \quad (1)$$

$$\frac{\partial \mathbf{B}^{(1)}}{\partial t} = -\nabla \times \mathbf{E}^{(1)}, \quad (2)$$

$$\frac{\partial \mathbf{E}^{(1)}}{\partial t} = \int d^3v \mathbf{v} \frac{f^{(1)}}{n_0} + \frac{c^2}{v_{T0}^2} \nabla \times \mathbf{B}^{(1)}. \quad (3)$$

We can simplify Eq. (1) noting that $\nabla_{\mathbf{v}} f^{(0)} = -\mathbf{v} f^{(0)}$, and therefore the term $\mathbf{v} \times \mathbf{B}^{(1)} \cdot \nabla_{\mathbf{v}} f^{(0)} = 0$. Furthermore, we can divide $f^{(1)}$ into an odd and even function of v yielding two equations:

$$\frac{\partial f_{odd}^{(1)}}{\partial t} + \mathbf{v} \cdot \nabla f_{even}^{(1)} + \mathbf{E}^{(1)} \cdot \mathbf{v} f^{(0)} = 0, \quad (4)$$

$$\frac{\partial f_{even}^{(1)}}{\partial t} + \mathbf{v} \cdot \nabla f_{odd}^{(1)} = 0. \quad (5)$$

Initially $f^{(1)}$ is even and proportional to x or y , and thus the gradient is uniform in space. Since the initial $E^{(1)}$ is either 0 or uniform, Eq. (4) shows that an odd function is produced, that is also uniform in space. Initially $E^{(1)}$, $B^{(1)}$, and $f_{even}^{(1)}$ do not change since $f^{(1)}$ is even, and $E^{(1)}$ and $B^{(1)}$ are uniform in space (see Eqs. (2, 3, 5)). Next, the new odd function generates an electric field seen in Eq. (3) which remains uniform in space. Moreover, since $f_{even}^{(1)}$ has not changed and the new $E^{(1)}$ is uniform in space, the $f_{odd}^{(1)}$ produced continues to be uniform in space (see Eq. (4)). $B^{(1)}$, and $f_{even}^{(1)}$

continue to not change since $f_{odd}^{(1)}$ and $E^{(1)}$ are uniform in space (see Eqs. (2, 3, 5)). At all subsequent times, the same arguments hold, and $f^{(1)} - f^{(1)}(t=0)$ will continue to be odd in v and uniform in space.

Note that additional factors of the Lorentz factor $\gamma = (1 - v^2/c^2)^{-1/2}$ found in the relativistic equations, or coupling to a similar Vlasov equation for an ion species, by an additional ion current in Eq. (3) proportional to c_s/v_{T0} do not affect these arguments, such that $f^{(1)}$ will continue to be odd in v and uniform in space. (Keep in mind, the ion distribution also evolves according to Eqs. (4–5).) Since the first order terms are all odd in v and uniform in space, we can thus safely conclude that the second order terms ($\sim \epsilon^2$) that are even in v or space dependent (which is in fact all of them) are only slightly modified by small c_s/v_{T0} and v_{T0}^2/c^2 terms $\sim \epsilon^0$.

Although the previous discussion has demonstrated that these small terms can be neglected, for completeness, we will also perform a similar analysis for the second order terms. Here we will demonstrate that it is required that none of the second order solutions are uniform in space unless they are also even with respect to v , or magnetic fields. For the second order terms:

$$\frac{\partial f^{(2)}}{\partial t} + \mathbf{v} \cdot \nabla f^{(2)} - \mathbf{E}^{(1)} \cdot \nabla_{\mathbf{v}} f^{(1)} + \mathbf{E}^{(2)} \cdot \mathbf{v} f^{(0)} = 0, \quad (6)$$

$$\frac{\partial \mathbf{B}^{(2)}}{\partial t} = -\nabla \times \mathbf{E}^{(2)}, \quad (7)$$

$$\frac{\partial \mathbf{E}^{(2)}}{\partial t} = \int d^3v \mathbf{v} \frac{f^{(2)}}{n_0} + \frac{c^2}{v_{T0}^2} \nabla \times \mathbf{B}^{(2)}. \quad (8)$$

Now we can divide $f^{(2)}$ into an odd and even function of v :

$$\frac{\partial f_{odd}^{(2)}}{\partial t} + \mathbf{v} \cdot \nabla f_{even}^{(2)} - \mathbf{E}^{(1)} \cdot \nabla_{\mathbf{v}} f_{even}^{(1)} + \mathbf{E}^{(2)} \cdot \mathbf{v} f^{(0)} = 0, \quad (9)$$

$$\frac{\partial f_{even}^{(2)}}{\partial t} + \mathbf{v} \cdot \nabla f_{odd}^{(2)} - \mathbf{E}^{(1)} \cdot \nabla_{\mathbf{v}} f_{odd}^{(1)} = 0. \quad (10)$$

Initially $f^{(2)}$ is even and proportional to x^2 or y^2 , and thus the gradient is proportional to x or y . Eq. (9) shows that since the initial $E^{(1)}$ is uniform, and the initial $E^{(2)}$

and $f_{\text{even}}^{(1)}$ are either 0 or proportional to x or y , an odd function is produced, that is proportional to x or y . From Eq. (8), $E^{(2)}$ does not change since $f^{(2)}$ is even, and $B^{(2)}$ is uniform. From Eq. (7), $B^{(2)}$ grows uniformly in space, because $E^{(2)}$ is proportional to x or y leading to a uniform gradient. Likewise $f_{\text{even}}^{(2)}$, from Eq. (10), grows uniformly in space, because $f_{\text{odd}}^{(1)}$ and $E^{(1)}$ are uniform.

After the initial stage, the new odd function generates an electric field seen in Eq. (8) which remains proportional to x or y , while the curl of $B^{(2)}$ remains 0. Moreover, since the additional $f_{\text{even}}^{(2)}$ is uniform and the new $E^{(2)}$ is proportional to x or y , the $f_{\text{odd}}^{(2)}$ produced continues to be proportional to x or y . $B^{(2)}$, and $f_{\text{even}}^{(2)}$ continue to grow uniformly since $f_{\text{odd}}^{(2)}$ and $E^{(2)}$ are proportional to x or y , and $f_{\text{odd}}^{(1)}$ and $E^{(1)}$ remain uniform. At all subsequent times, the same arguments hold, and the $E^{(2)}$ and $f_{\text{odd}}^{(2)}$ produced are all proportional to x or y , while the $B^{(2)}$ and $f_{\text{even}}^{(2)}$ produced are all uniform in space. Again this analysis was for the sake of completeness, but it further justifies neglecting the small terms c_s/v_{T0} and v_{T0}/c .

In order to find the explicit time dependence of $E^{(1)}$, $E^{(2)}$, $B^{(2)}$, $f_{\text{odd}}^{(1)}$, $f_{\text{odd}}^{(2)}$, and $f_{\text{even}}^{(2)}$, we assume the initial condition of $f = f_0$, no initial electric or magnetic fields (or guess an equilibrium field), and take an expansion for small $t\omega_{pe}$. For example we can use Eq. (2) to find $f_{\text{odd}}^{(1)}$ to first order in $t\omega_{pe}$, then Eq. (3) to find $E^{(1)}$ and Eq. (2) to find $f_{\text{odd}}^{(1)}$ to second order in $t\omega_{pe}$, and continue to higher orders in $t\omega_{pe}$. Fortunately, summing over all orders of t converges to an analytic solution valid for $t \sim \epsilon^0$. The same procedure is used to calculate the second order terms in ϵ .

II. DENSITY GRADIENT.

We first consider the case with only a density gradient ($\delta = 0$). If we assume the initial condition of $f = f_0$ and no initial electric or magnetic fields, the solution to the Vlasov Maxwell's equation was described as:

$$f = f_0 + \tilde{f}_n(t). \quad (11)$$

Here the oscillatory term is defined as:

$$\begin{aligned} \tilde{f}_n(t) \equiv & -\epsilon \sin(\omega_{pe,x}t) v_x f_M \\ & + \frac{1}{2} \epsilon^2 \sin(\omega_{pe,x}t) x v_x f_M \\ & - \epsilon^2 [1 - \cos(\omega_{pe,x}t)] v_x^2 f_M \\ & + \frac{1}{2} \epsilon^2 t \sin(\omega_{pe,x}t) v_x^2 f_M \\ & - \frac{1}{2} \epsilon^2 [1 - \cos(\omega_{pe,x}t)]^2 (v_x^2 - 1) f_M, \quad (12) \end{aligned}$$

where $\omega_{pe,x} \equiv 1 + \epsilon x/2$ is the normalized plasma frequency based on the x dependent density, n . Note that we have made use of the Poincaré-Lindstedt method [1, 2], which by modifying the frequency in the solution, avoids unphysical secularly growing terms. This is done by including additional higher order terms ($> \epsilon^2$) found in the expansion of the sin and cos terms.

The third and last terms on the RHS of Eq. (12) are associated with a modification to the density, temperature, and temperature anisotropy of the plasma. Although a component of each of these terms does not oscillate with time, these terms are insignificant because this modification is of order ϵ^2 , and does not grow with time.

Despite the use of the Poincaré-Lindstedt method [1, 2], which avoids unphysical secularly growing terms, there still exists a secular term in f , which grows linearly with time until $t \sim \epsilon^{-1}$ where the assumptions of the ordering break. Thus our model is only valid as long as t remains small compared to this limit. This term is, however, physical, and represents the increasing electron density associated with the divergence of the electric field:

$$\begin{aligned} \nabla \cdot \mathbf{E} &= (n_i - n_e)/n_0 \\ &= \epsilon^2 \left[1 - \cos(\omega_{pe,x}t) - \frac{1}{2} \omega_{pe}t \sin(\omega_{pe,x}t) \right]. \quad (13) \end{aligned}$$

This increasingly large divergence is caused by the space dependent frequency, $\omega_{pe,x}$, which gives rise to increasingly shorter scale variations along x in the electric field. These variations along x lead to phase mixing and Landau damping. At late time, where the assumptions break down, Landau damping eventually eliminates both the oscillations and the secular term.

In the case where there is an initial electric field such that there are no oscillatory terms,

$$\nabla \cdot \mathbf{E} = \epsilon^2, \quad (14)$$

so there is only a slight constant and uniform difference between n_i and n_e .

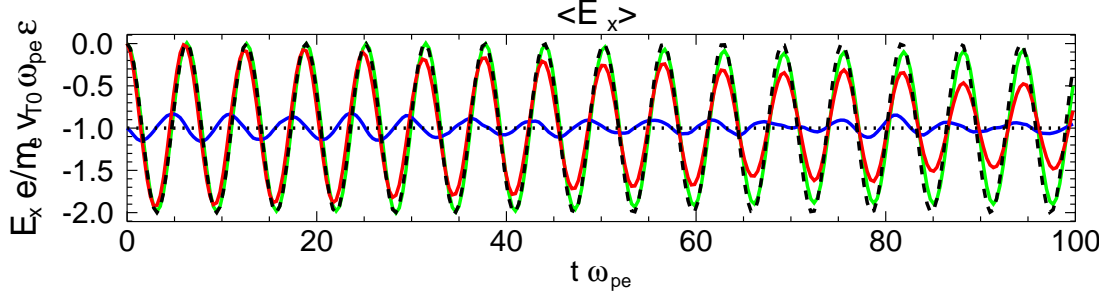


FIG. 1. Average E_x vs. time due to the density gradient starting from 0 electric field (red), and starting from Eq. (17) (blue), along with the predicted curves from Eqs. (19, 17) (black dashed/dotted lines respectively). Average E_x starting from $\mathbf{E} = 0$ between $x/\lambda_D = -10, 10$, and $y/\lambda_D = -490, 490$, with 64,000 ppg (green) instead of 8,000 ppg.

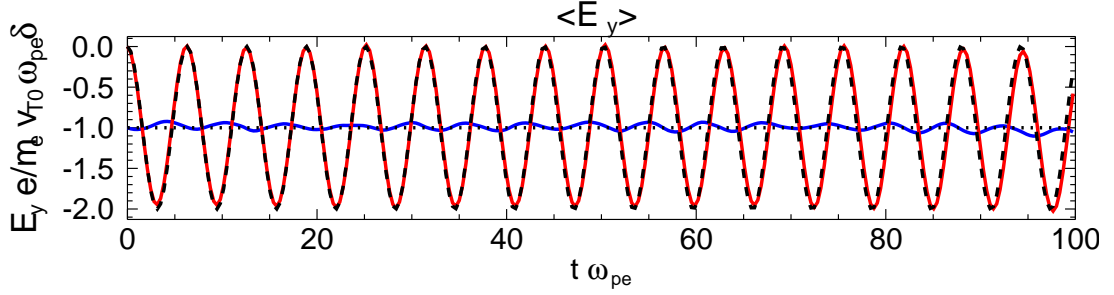


FIG. 2. Average E_y vs. time due to the temperature gradient starting from 0 electric field (red), and starting from Eq. (18) (blue), along with the predicted curves from Eqs. (20, 18) (black dashed/dotted lines respectively).

III. TEMPERATURE GRADIENT.

We now consider the second case, with only a temperature gradient ($\epsilon = 0$). If we again assume the initial condition of $f = f_0$ and no initial electric or magnetic fields, the solution to the Vlasov Maxwell's equation was described as:

$$f = f_{\nabla T} + \tilde{f}_T(t). \quad (15)$$

Here the oscillatory term is defined as:

$$\begin{aligned} \tilde{f}_T(t) \equiv & -\delta \sin(t) v_y f_M \\ & + \frac{1}{2} \delta^2 \sin(t) y (5 - v^2) v_y f_M \\ & - \frac{1}{2} \delta^2 [1 - \cos(t)] (5 - v^2) v_y^2 f_M \\ & + \frac{1}{2} \delta^2 [1 - \cos(t)] [v_y^2 (7 - v^2) - (5 - v^2)] f_M \\ & - \frac{1}{2} \delta^2 t \sin(t) [v_y^2 (7 - v^2) - (5 - v^2)] f_M \\ & - \frac{1}{2} \delta^2 [1 - \cos(t)]^2 (v_y^2 - 1) f_M. \end{aligned} \quad (16)$$

Like the previous case, there is a term proportional to t in the distribution function $\tilde{f}_T(t)$, which eventually

breaks the assumptions of the ordering. However, while the assumptions hold, this term is not so significant as it does not contribute to either the temperature, or the density of the system.

In addition, the third and last terms on the RHS of Eq. (16) are associated with a modification to the density, temperature, and temperature anisotropy of the plasma, that does not oscillate with time. However, these terms are also insignificant because this modification is of order δ^2 , and does not grow with time.

In a system with a density gradient, both these oscillations, and those found in the electric field would Landau damp as described earlier.

IV. NUMERICAL COMPARISON.

Our theoretical model has been tested via particle-in-cell (PIC) simulations using the OSIRIS framework [3, 4], and we have obtained agreement with the predicted anisotropic heating and magnetic field generation. Here we will explain our initial setup and parameters, as well as show further agreement with our model.

Unless otherwise specified, the simulations are performed with the parameters $L_T/\lambda_D = L_n/\lambda_D = 1000 =$

ϵ^{-1} , and a box half width of $L_x/\lambda_D = 49$, and $L_y/\lambda_D = 490$. The normalized thermal velocity has been chosen small, $v_{T0}/c = 0.05$, such that relativistic effects do not play a role, but it is large compared to $\epsilon = 0.001$. At the ends of the density gradient the particles have reflecting boundary conditions, and at the ends of thermal gradient there is a thermal bath. On all sides there are magnetic conducting boundary conditions. The box is longer in the y direction to isolate the central region of the simulation from possible non-physical boundary effects due to the thermal bath. Our simulations run until $\omega_{pe}t = 100$, while $\omega_{pe}L_y/v_{T0} = 490$. The resolution is 1.4 grid points per Debye length (λ_D) and the time resolution is $\Delta t\omega_{pe} = 0.0175$. In order to resolve the small order details, we use a large number of particles per grid cell (ppg) of 8,000. All of the presented simulations are done with non-moving ions like assumed in the calculation.

To test these solutions we look at both simulations with $\delta = 0$ or $\epsilon = 0$, (periodic boundary conditions in the direction with no gradient), and with both gradients.

Here we further test the model by examining the equilibrium static electric fields in the cases with $\delta = 0$ predicted to be:

$$\mathbf{E} = -(\epsilon - \epsilon^2 x) \hat{\mathbf{x}}, \quad (17)$$

and for $\epsilon = 0$:

$$\mathbf{E} = -\delta \hat{\mathbf{y}}, \quad (18)$$

and for oscillatory electric fields generated when the initial electric field is zero, in the cases with $\delta = 0$:

$$\mathbf{E} = -(\epsilon - \epsilon^2 x) [1 - \cos(\omega_{pe,x}t)] \hat{\mathbf{x}}, \quad (19)$$

and for $\epsilon = 0$:

$$\mathbf{E} = -\delta [1 - \cos(t)] \hat{\mathbf{y}}. \quad (20)$$

In Fig. 1, one can see the oscillations in the average electric field from the simulation with $\delta = 0$ following

Eq. (19). The decay in amplitude is an effect of the averaging with $\omega_{pe,x}$, which is a function of x , and so a simulation with a smaller range in x/λ_D (-10,10) from a simulation with better statistics (64,000 ppg) is also shown for comparison. In a simulation starting with Eq. (17), the electric field stays at the equilibrium value. Similarly, in Fig. 2 the oscillations in the electric field from the simulation with $\epsilon = 0$ follow Eq. (20), and a simulation starting with Eq. (18), shows the electric field staying at the equilibrium value.

In the case with both gradients, since the boundary conditions significantly affect the magnetic fields close to the boundaries (at the boundary $B_z = 0$), it was necessary to further increase the box size by a factor of 10 in the y direction. The ordering assumptions are only met where $x/\lambda_D \sim \epsilon^0$, and a simulation where this is true for a significant range would be unfeasible. The fields are calculated by averaging the results between $-49 < x/\lambda_D < 49$, and $-49 < y/\lambda_D < 49$. For the simulation with both $\delta \neq 0$ and $\epsilon \neq 0$, similar curves with constant electric fields as shown in blue in Figs. (1–2) were obtained.

V. ACKNOWLEDGMENTS.

This work was supported by the European Research Council (ERC-2010-AdG Grant No. 267841, and ERC-2015-AdG Grant No. 695008). NFL was partially funded by NSF CAREER award no. 1654168.

-
- [1] A. Lindstedt, Abh. K. Akad. Wiss. St. Petersburg **31** (1882).
 - [2] H. Poincaré, *Les Méthodes Nouvelles de la Mécanique Céleste, II [1882]* (Dover Publ., New York, 1957).
 - [3] R. A. Fonseca, L. O. Silva, F. S. Tsung, V. K. Decyk, W. Lu, C. Ren, W. B. Mori, S. Deng, S. Lee, T. Katsouleas, and J. C. Adam, Lect. Notes Comput. Sci. **2331**, 342 (2002).
 - [4] R. A. Fonseca, S. F. Martins, L. O. Silva, J. W. Tonge, F. S. Tsung, and W. B. Mori, Plasma Phys. Contr. Fusion **50**, 124034 (2008).